Bi-Axial Growth Mode of Au−TTF Nanowires Induced by Tilted Molecular Column Stacking

Yanlong Xing,[†,⊥] Eugen Speiser,*[,†] Dheeraj K. Singh,[‡,§] Petra S. Dittrich,[∥] and Norbert Esser[†]

[†]Leibniz-Institut für Analytische Wissenschaften-ISAS-e.V., 12489 Berlin, Germany
[⊥]School of Chemical and Environmental Engineering, Shandong University of Science and Technology, 266590 Qingdao, PR China
[‡]Department of Chemical Physics, Jacobs University, 28759 Bremen, Germany
[§]Department of Physics, Institute of Infrastructure Technology Research & Management, 380026, Ahmedabad, India
[∥]Department of Biosystems Science and Engineering, ETH Zurich, 4058 Basel, Switzerland

S *Supporting Information*

ABSTRACT: In this study, to understand the molecular self-organization in metal−organic charge-transfer nanowires, single gold-tetrathiafulvalene (Au−TTF) nanowires were analyzed using polarized Raman spectroscopy, combined with density functional theory (DFT) calculations. To verify the methodology, an investigation was done for neutral tetrathiafulvalene (TTF) bulk crystals with well-known structure. On the basis of the DFT calculation of the molecular Raman tensor and simulation of the angular-dependent depolarization ratio, the molecular orientation in single TTF crystals was verified. Thereon, the combined experimental and ab initio-simulation method was applied to study single Au−TTF nanowires. Our results clearly demonstrate, in contrast to the commonly accepted parallel molecular stacking model, that at least two molecules with different orientations are located in the unit cell of the nanowire's crystal structure. The new tilted molecular column stacking wire model explains also the axial and radial growth mechanism of Au−TTF wires.
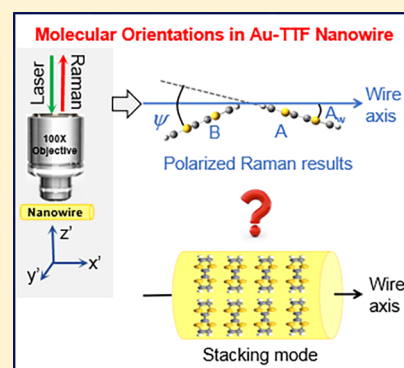
1. INTRODUCTION

Metal−organic charge transfer nanowires have drawn significant attention due to their conductive characteristics, tunable properties, and their integration in microfluidic devices.[1−3] Au−TTF is formed by the reaction between chloroauric acid and TTF. It has been proven for high electronic conductivity,[1] microfluidic-integrated synthesis,[1] and applications in sensing.[4,5] Since their discovery, Au−TTF wires were reported to have uniform 1D morphology and the formation mechanism was thought to be based on the aggregation of parallel, columnar stacking of neutral and charged TTF molecules in perpendicular orientation to the growth direction. It was also claimed that the self-assembly of gold nanoclusters on the surface of the nanowire produced from the redox reaction inhibits nanowire lateral growth.[6]

However, we observed that Au−TTF forms wires with diameters in nanometer to micrometer scale, tuned by the reaction conditions, e.g., microfluidic flow rates or reaction time.[1,5] Therefore, the lateral growth is not inhibited by gold nanoclusters. In this case, it is difficult to understand the variation of wire diameters by the parallel columnar stacking model. The stacking and orientation of TTF molecules is of great importance for understanding the growth mechanism and the electronic structure of Au−TTF and related materials, as well as the influence of the adsorbents on the surface (sensor applications). Therefore, a detailed nondestructive structure analysis of single Au−TTF wires was performed using Raman spectroscopy.

Polarized Raman spectroscopy is known to be an efficient technique to study the molecular ordering in crystals or organic thin films.[7−10] Combined with confocal microscopy, polarized Raman spectroscopy has also been employed to study nanostructures.[11−13] In the present study, this technique was applied for the first time to study single TTF-based metal−organic nanowires, to the best of our knowledge. Aiming to verify the analytical approach based on Raman scattering combined with ab initio-simulations, we first investigated a single TTF crystal with known crystal structure. The rotation angles of the molecules related to the crystal axes were determined by polarized Raman spectroscopy using calculated Raman tensor elements of TTF molecules. Upon rotation of polarization of incident and scattered light on different facets of the crystal, the periodically varying Raman intensity was observed. The depolarization ratio (P, eq S1, Supporting Information is a useful quantity to determine the molecular orientations in an ordered molecular crystal.[7,14] On the basis of the simulation of the depolarization ratio, the known TTF assembly in a single crystal[15] was confirmed. The same analysis method was subsequently applied to study various single Au−TTF nanowires synthesized in microchannels.[1]
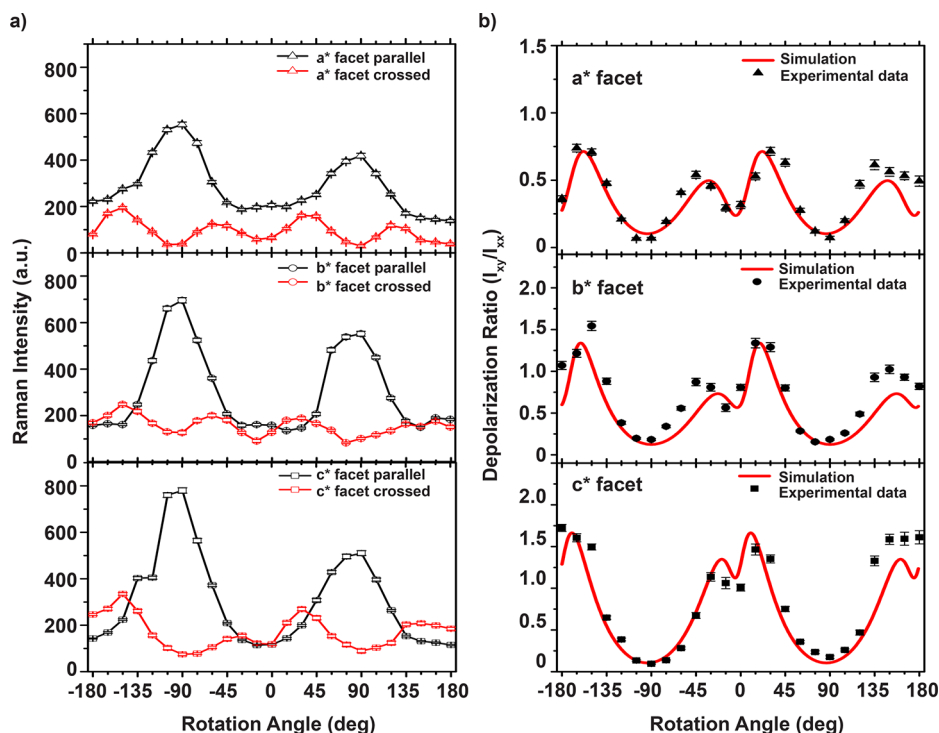
Figure 1. (a) Polarization dependence of the Raman intensity of the 1516 cm^{-1} A$_g$ vibration measured from different facets (a*, b*, c*, see Figure S4a) of the TTF crystal under parallel (black hollow symbol) and crossed (red hollow symbol) polarization configuration. The spectra are shown in Figure S5 (Supporting Information). (b) Experimental (black solid symbols) and simulated depolarization ratio (red lines) of the A$_g$ mode at ~1516 cm^{-1}, obtained upon rotation around the normal of the three facets of a TTF crystal. Red lines are the simulation with a finite polarization uncertainty (D ∼ 0.08). The Pearson correlation coefficients between fitted red lines and experimental data are 0.804, 0.843, and 0.851 for a*, b*, and c* facets, respectively.

2. EXPERIMENTAL AND COMPUTATIONAL METHODS

2.1. Chemicals. Acetonitrile (CH$_3$CN, 99.8+%) and *n*-heptane (99.7+%) were purchased from Merck (Gernsheim, Germany). Gold(III) chloride trihydrate (HAuCl$_4$, 99+% trace metal basis) was purchased from Sigma−Aldrich (Munich, Germany). TTF (>98.0%, GC) was obtained from TCI (Eschborn, Germany).

2.2. Synthesis. Single TTF crystals were grown by recrystallization of commercially obtained TTF samples which were dissolved in hexane (saturated solution),[10,16] which resulted in bright orange needles, up to 2 cm long and about 0.25 mm^2 in cross section (Figure S1a) and exhibited flat facets. A single TTF crystal was selected under a microscope and rotated for polarized Raman spectroscopy measurement on different facets at room temperature. Different diameters of Au−TTF wires were synthesized on four-inlet microchips by controlling the flow rates of reactants[1] (Figure S1b−f, Supporting Information).

2.3. Raman Measurement. The polarized confocal Raman microscopy analysis was carried out on an in-house assembled confocal Raman microscope equipped with a diode-pumped solid-state (DPSS) laser (Cobolt Samba, λ = 532 nm), and a liquid N$_2$ cooled CCD as detector. The spectral resolution is around 2 cm^{-1}. The ingoing polarization controlled using the intrinsic laser polarization and a half-wave plate. Focusing on the sample was done with a 50× objective (Olympus MPL, NA = 0.75, for TTF crystals) and a 100× objective (Zeiss EC Epiplan-NEOFLUAR, NA = 0.70, for Au−TTF). Different laser intensities were applied for TTF crystals and Au−TTF wires, in order to obtain the optimal Raman response. The laser intensity was about 15 μW at the focal point for the analysis of TTF crystals with an acquisition time of 120 s per spectrum. For

Au−TTF wires, a low laser intensity (about 7 μW) and an acquisition time of 60 s per spectrum were applied. The Raman signal was collected under a backscattering geometry. A half-wave plate served to carry out the angular polarization rotation with respect to the wire structures. The angle of the polarized incident light was varied in the range of −180° to +180° by rotating the half-wave plate with the angle within 0−180°. In addition, a polarizer served as an analyzer just in front of the entrance slit of the spectrometer. Two polarization configurations (parallel and crossed) were applied in this work. The polarization analyzer was rotated by 90° to select crossed configuration.

2.4. DFT Calculation. In this work, the DFT calculations were used to obtain the exact values of the Raman tensor elements of TTF molecules (neutral and TTF cation). The calculations were carried out using the B3LYP level of theory supplemented with the standard 6-31+G(d,p) basis set and the Gaussian 09 program package.[17] The geometry optimization and harmonic Raman frequencies of the different normal modes of neutral TTF (C$_{2v}$ point group) and TTF cations (D$_{2h}$ point group) were calculated using DFT. In order to get the Raman tensor element, the quadrupole moment was taken into account using the polar keyword in DFT calculations. The global minima on the potential energy surface were confirmed by the real harmonic vibrational wavenumbers calculated for both neutral TTF (C$_{2v}$ point group) and TTF cation (D$_{2h}$ point group). In the studies reported recently, DFT calculations with B3LYP method[13,14,18−20] provided useful results for understanding the observed phenomenon (e.g., self-association and hydrogen bonding in molecules, molecular vibration).

Table 1. DFT Calculation: Structure and Raman Tensor Elements of TTF^0 and TTF^+ [a]

Molecule	Point group	DFT model[#]		Traceless quadrupole moment (field-independent basis)*		
		Top view	Side view	a	b	c
TTF^0	C_{2v}			-5.0235	16.8375	-11.814
TTF^+	D_{2h}			-24.3185	-7.8936	32.2121
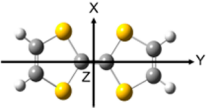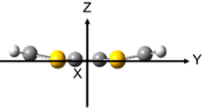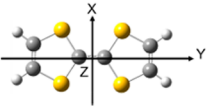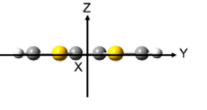
[a]Key: (#) DFT modeling of TTF^0 and TTF^+. Yellow, dark gray and light gray balls represent S, C and H, respectively. XYZ are the molecular coordinates. (∗) Calculated Raman tensor elements of TTF^0 and TTF^+. The Raman tensor elements (a, b, c) refers to A_g modes in Table S1 (Supporting Information)

2.5. Simulation. The simulation of the depolarization ratio was done according to eqs 1, 2, and S2–S4. The fitted curves of the depolarization ratio (red lines in Figure 1b, Figure 3, and Figure S9 (Supporting Information)) were obtained by the results with the optimized correlation.

2.6. Single TTF Crystal Analysis. Crystal data were obtained from the Cambridge Structural Database (reference code BDTOLE 10) and analyzed by the Mercury 3.6 software, which was downloaded from the Cambridge Crystallographic Data Center. Calculations of molecular planes and angle measurements were carried out using the "Calculate planes" and "Picking mode: Measure Angles" tools implemented in the software.

2.7. Raman Spectra Analysis. All Raman spectra were baseline-corrected. The peak positions and intensities were fitted by the Lorenz algorithm (Origin 9.0 Pro software) in the range from 1100 to 1700 cm^{-1}.

3. RESULTS AND DISCUSSION

3.1. DFT Calculation of Raman Tensor Elements. To investigate the molecular orientation by the Raman depolarization ratio, the Raman tensor elements of neutral TTF and charged TTF^+ molecules were calculated by DFT for the A_g modes. Optimized molecular structures of isolated TTF and TTF^+ molecules are shown in Table 1. The neutral TTF molecule has a nonplanar boat-like structure with C_{2v} symmetry, whereas the TTF cation shows a D_{2h} symmetry planar structure balanced by a positive charge transfer.[21] The calculated structures are in accordance with previously reported work.[19] The Raman tensors for C_{2v} (TTF neutral) and D_{2h} (TTF cation) isomeric point groups, based on the molecular symmetries,[7] are shown in Table S1 (Supporting Information). Tensor elements (a, b, c) calculated for both TTF and TTF^+ are also depicted in Table 1.

3.2. Polarized Raman Spectra of Single Bulk TTF Crystals. Molecular orientations in single TTF crystals derived from Raman measurements and simulations based on DFT Raman tensor calculations were compared with the reported single crystal structure from X-ray analysis. Since TTF crystal exhibits the monoclinic α-TTF phase at room temperature (Figure S2, Supporting Information)[15,16] which was intensively studied by Cooper et al. in early 1970s,[8,22] we use this crystal structure with two molecules in the elementary cell for the

evaluation of our method. The angle between the two molecule planes (S1–S2–C3–C3B–S2B–S1B plane in Figure S3, Supporting Information) from reported work (52.59o in Figure S2, Supporting Information) was used as a criterion for the validity of our approach.

Polarized Raman measurements were carried out on a single TTF crystal which has three facets (a*, b*, c*), with the laser beam at near-normal incidence in the x, y, z directions (Figure S4a, Supporting Information) in backscattering geometry, under parallel and perpendicular configurations. The spectrum of a TTF crystal (from the a* facet at room temperature) shows typical Raman peaks at 315, 471, 795, 1089, and 1516 cm^{-1} (Figure S4b, Supporting Information) which belong to A_g vibrational modes, while the peak at 58 cm^{-1} belongs to a B_g vibrational mode.[16,20]

Raman spectra from facets a*, b*, and c* under parallel/crossed polarization are shown in Figure S5a–f (Supporting Information). Upon rotation of the polarization of the incoming laser, the Raman intensity of the A_g vibrational modes changes with a periodicity of 180° and 90° under parallel and crossed polarization configurations, respectively (black and red lines in Figure S5, Supporting Information). This suggests a preferential orientation of TTF molecules in the crystal. The intensities of the A_g mode at ∼1516 cm^{-1} (out-of-phase vibrational of all C=C bonds, Figure S3b, Supporting Information) were used for a quantitative structure analysis.

On the basis of the Raman intensities from spectra at the three facets of TTF crystal as a function of polarization rotation (Figure 1a), the depolarization ratio $\acute{P}$ was calculated (Figure 1b, symbols) and simulated (Figure 1b, red lines) according to eq 1,[7]

$$P' = \frac{(1 - D)I_{xy} + D \times I_{xx}}{D \times I_{xy} + (1 - D)I_{xx}} \tag{1}$$

Here, the intensities of scattered light polarized in parallel (I_{xx}) and perpendicular (I_{xy}) configurations were corrected in order to consider the limited degree of polarization due to surface roughness and instrumental polarization errors by a constant factor D.[7] For the simulation of the depolarization ratio, a two-molecule system was used according to the α-TTF bulk crystal structure (see Figure S2, Supporting Information). To describe the molecular orientations with respect to crystal axes, three

angles (Euler's angles, typically denoted as α, β, γ) are employed.[23]

3.3. Simulation of Depolarization Ratio. The experimental and simulated depolarization ratios of the 1516 cm^{-1} peak under angular variation of three facets (a^*, b^*, c^*, see Figure S4a) are shown in Figure 1b. The red lines are the simulated depolarization ratio for the three facets with fitted Euler angles and angle between two molecules in the unit cell. The simulation of the Raman intensity (I_{is}) is dependent on the polarization of the incoming (e_i) and scattered light (e_s) and the molecular orientation (α, β, γ) eq 2:

$$I_{is} \propto e_i \cdot M_{zxz}^T(\alpha, \beta, \gamma) \cdot \overline{\overline{R}}(\psi) \cdot M_{zxz}(\alpha, \beta, \gamma) \cdot e_s \qquad (2)$$

where $M_{zxz}(\alpha, \beta, \gamma)$ represents the Euler rotation matrix and $\overline{\overline{R}}(\psi)$ is the Raman tensor while ψ is the angle between the two molecules rotated around the molecular X axis (see Table 1). The Raman intensities under parallel (I_{xx}) and crossed (I_{xy}) configurations are related to the Raman tensor and the rotation described by the Euler angles (see eqs S2–S4, Supporting Information).

The orientation of the TTF molecules and the angle between the two molecular planes in the crystal were obtained from the simulation of the depolarization ratio (Figure 1b). A high correlation between experimental data and simulated results from three different facets of the crystal was obtained.

The angle between two molecules was calculated from different facets as 51.4° (a^* facet), 51.6° (b^* facet), and 51.8° (c^* facet) (Table S2, Supporting Information). All of these angles are in the range of 51.6° ± 0.2°, indicating a close agreement with the angle of the single crystal structure[8] (52.59°, Figure S2, Supporting Information). Thus, the combined experimental and ab initio-simulation method was proven to be an efficient tool to study the molecular structure of TTF-based materials.

3.4. Polarized Raman Spectra of Individual Au–TTF Nano- and Microwires. Subsequently, the above-mentioned method was applied to the analysis of various single Au–TTF nanowires (diameters 630 ± 130 nm; Figure S1b, Supporting Information) and microwires (diameters 1–4 μm; Figure S1b–f, Supporting Information). First, the polarized Raman spectra of single Au–TTF nanowires under parallel and crossed polarization configurations were obtained. The Raman peaks (A$_g$ modes) for the partially charged TTF^{n+} ($0 < n < 1$) molecules in the nanowire are shifted from those of neutral TTF molecules (Figure S4b), yielding modes of 504 cm^{-1} (in-plane vibration), 753 cm^{-1} (C–S stretching), 1011 cm^{-1} (C–H in-plane bend), 1369 cm^{-1} (C–C stretching + C–H bend), 1415 cm^{-1} (central C=C bond stretching) and 1513 cm^{-1} (ring C=C stretching) (Figure 2). The Raman mode assignments of TTF, TTF^{n+} ($0 < n < 1$) and TTF$^+$ are listed in Table S3 (Supporting Information). Strong shifts are found in the A$_g$ peak positions between neutral and charged TTF, while similar peak positions were observed for partially charged TTF^{n+} ($0 < n < 1$) and fully charged TTF cations. Spectra for the polarization configurations ($Z'(Y'Y')\overline{Z}'$ and $Z'(X'X')\overline{Z}'$, Figure 2) with polarization parallel and perpendicular to the nanowire axes were different, showing that TTF molecules were assembled in a certain defined orientation within the wire.

Following, the polarization dependent Raman spectra of Au–TTF were obtained upon rotation of the incoming laser polarization in steps of 15°. As shown in Figure S6 (Supporting Information), the Raman intensities of the A$_g$ modes (~1415
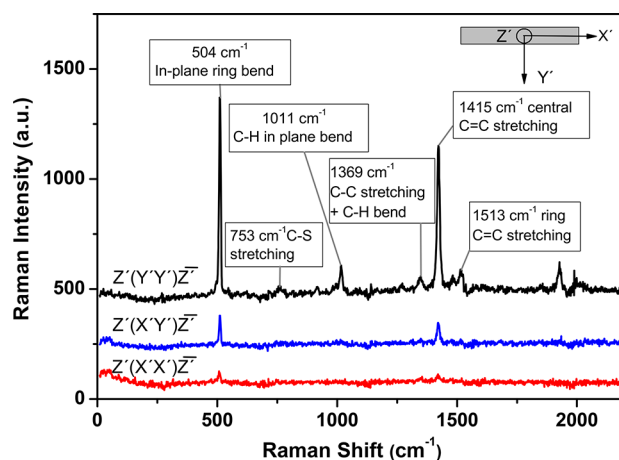
Figure 2. Raman spectra of a single Au–TTF wire under parallel (black and red spectra) and crossed (blue spectrum) polarization configurations. The full spectrum under $Z'(Y'Y')\overline{Z}'$ configuration shows the typical Raman active vibrations of TTF^{n+} ($0 < n < 1$). The figure inset indicates the definition of X'Y'Z' directions for a single wire. $\overline{Z}'$ refers to the direction of backscattered light.

cm^{-1}) varied with a period of 180° in parallel polarization ($Z'(X'X')\overline{Z}'$, Figure S6a), and 90° in crossed polarization configuration ($Z'(X'Y')\overline{Z}'$, Figure S6b, Supporting Information). The highest Raman signal in parallel polarization was obtained when the incoming laser polarization was perpendicular to the longitudinal axis of the wire. To study the depolarization ratio of Au–TTF nanowire systematically, six nanowires from different batches of synthesis were randomly selected for polarized Raman analysis. The A$_g$ mode vibration of the central C=C bond stretching was used for the quantitative analysis. Thus, the Raman intensities of peaks at 1415 cm^{-1} for the six different wires under parallel (I_{xx}) and crossed (I_{xy}) configurations (Figure S7, Supporting Information) were used for the analysis and modeled by the depolarization ratio with the calculated Raman tensor elements of the TTF cation (Table 1). Both experimental (symbols) and simulated (lines) results upon angular variation are shown in Figure 3. Here, a D value of ~0.08 was applied for all fitting curves. In an attempt to simulate the experimental results, a one-molecule model as assumed in the commonly accepted structure mode (simply parallel stacking mode)[6] was first applied. However, the simulation (blue line, Figure 3) showed a large deviation to the experimental results, implying that the partially charged TTF^{n+} ($0 < n < 1$) molecules were not all oriented in the same direction. Alternatively, when a two-molecule model was introduced, a much higher correlation of the simulation (red line, Figure 3) with the experimental results was achieved.

Apart from the above results obtained for the nanowires, four different microwires (Figure S1b–f, Supporting Information) were studied for comparison. On the basis of the angular dependent Raman intensity of A$_g$ mode at ~1415 cm^{-1} for these microwires under parallel (I_{xx}) and crossed (I_{xy}) configurations (Figure S8, Supporting Information), the depolarization ratio was calculated and simulated. The results indicated that a two-molecule simulation correlates well with the experimental results, in contrast to the one-molecule simulation (Figure S9, Supporting Information). These results are fully consistent with those in the simulation of Au–TTF nanowires (Figure 3).

These results suggest clearly that there were at least two different molecular orientations in all single nano/microwires
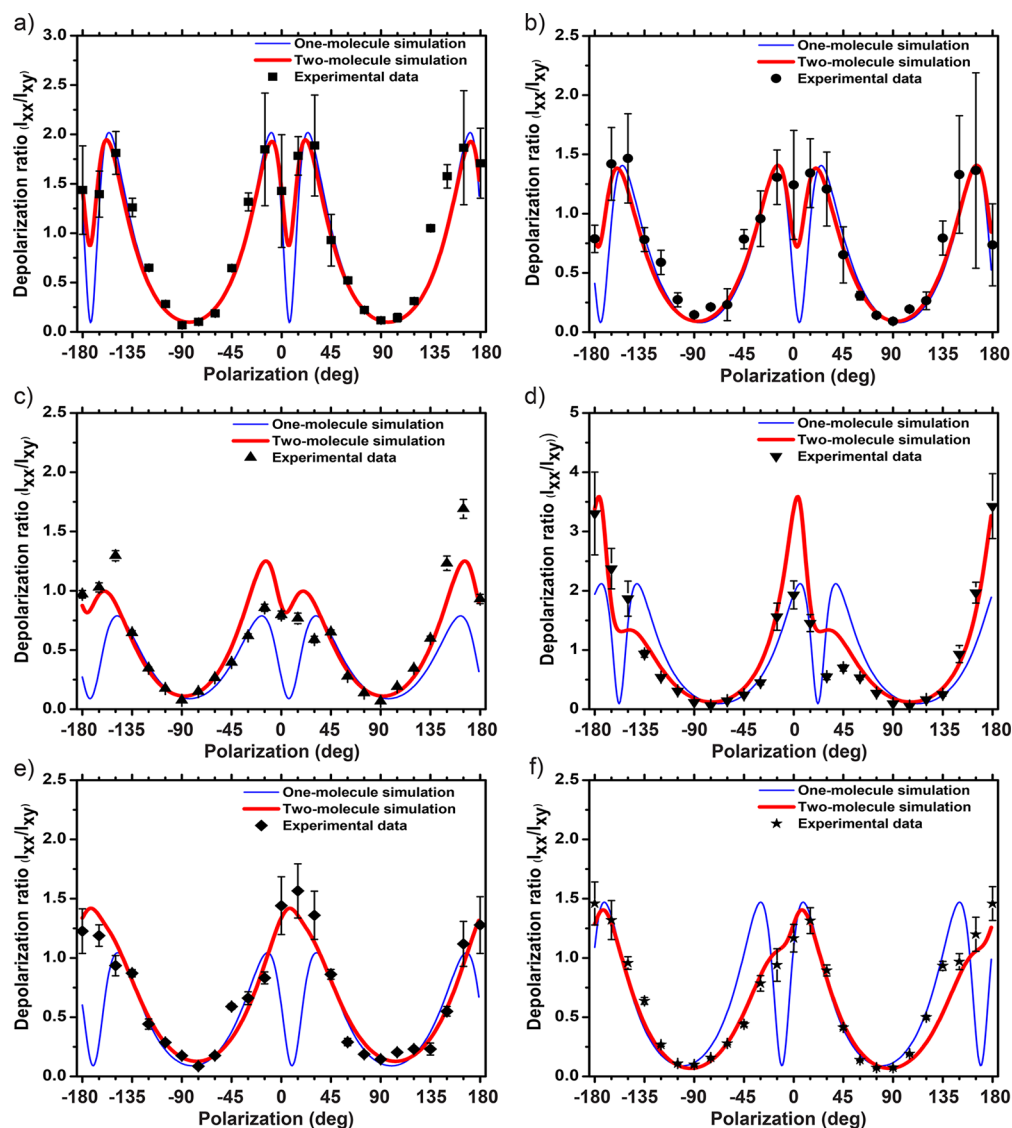
Figure 3. Depolarization ratio of six different Au−TTF nanowires. Experimental (symbols) and simulated (lines) depolarization ratio of the Raman intensity of the ~1415 cm^{-1} (central C≡C bond stretching) vibration obtained upon rotation of incoming and scattered polarization orientation around the Z′ axis of Au−TTF wires (Figure S7, Supporting Information). The blue lines are the one-molecule simulations, while the red lines are the two-molecule simulations. The X′Y′Z′ configurations refer to the inset in Figure 2. The Pearson correlation coefficients between fitted two-molecule lines (red) and experimental data are 0.937 (a), 0.911 (b), 0.794 (c), 0.863 (d), 0.929 (e), and 0.937 (f).

Table 2. Results Derived from the Two-Molecule Simulation of the Depolarization Ratio of Different Au−TTF nanowires

no.	α [deg]	β [deg]	γ [deg]	D	ψ [deg]	A_w [deg]
a	−135.2	152	137.8	0.084	54.0	18.76
b	45.6	153.4	138	0.074	53.4	20.45
c	49.6	154.2	138.4	0.082	53.2	20.44
d	−131.6	152.2	133.6	0.086	53.1	19.48
e	42.2	156	135.4	0.082	54.8	20.12
f	36.2	157.2	134.6	0.082	54.8	20.12
av angle					53.9 ± 1.6	19.9 ± 1.3

investigated. Using the two-molecule simulations, the angle between the two molecules was determined from the average fitted parameter ψ to be 53.9 ± 1.6° for nanowires (Table 2) and 53.4 ± 4.5° for microwires (Table S4, Supporting Information), indicating essentially the same two-molecule configurations in both Au−TTF nano- and microwires. An interesting observation is that the angular based depolarization ratio of the various nanowires (experimental data, Figure 3) and microwires

(experimental data, Figure S9, Supporting Information) exhibited different variations. This is because the wires were randomly rotated along their long axes when deposited on the glass slides before Raman measurements.

In the two-molecule simulation, we defined the molecules as A and B in a unit cell, where molecule A was oriented first by the Euler's angles derived from simulation and molecule B oriented according to the angle (ψ) between B and A. The simulated

Molecular Orientations of Au-TTF Nanowire and TTF Crystal
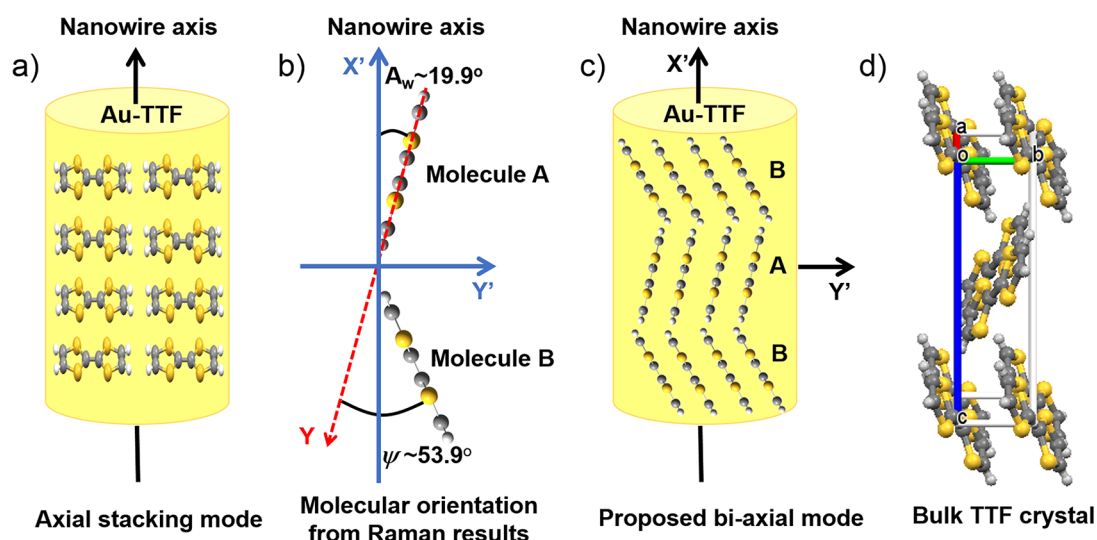
Figure 4. (a) Orientation of partially charged TTF^{n+} ($0 < n < 1$) molecules in the previously proposed structure.[6] (b) Molecular orientation from Raman results (2D view of Au−TTF nanowire model), with angle A_w (the angle between molecules A (Y axis) with wire axis X') and ψ (the angle between molecules A and B), Y' is the radial growth direction. (c) Biaxial stacking mode of Au−TTF nanowire derived in this work. The stacking can take place along X' and Y' directions. d) The molecular configuration of TTF neutral molecules in the unit cell of TTF crystal (view from the a axis of the unit cell).

results of the six different Au−TTF nanowires are shown in Table 2, including the Euler angles (α, β, γ), polarization error D, angle between two molecule planes (ψ) and the angle of molecule A with respect to the longitudinal axis of the wire (A_w). On the basis of the simulation of the different Au−TTF microwires, the A_w angle for microwires is calculated to be $20.2 \pm 0.3°$ (Table S4, Supporting Information), which is close to the A_w angle of nanowires ($19.9 \pm 1.3°$, Table 2). These results, together with the similar two-molecule configurations and the ψ angles between molecules, clearly proved that Au−TTF nano/microwires are both based on the same molecular structure.

3.5. Structure Model of Au−TTF Nanowires. We note that the molecular orientation obtained on all studied wires is in very close agreement with each other (Table 2 and Table S2, Supporting Information), which further indicates that the fitting method applied in the present work is reliable. On the basis of the simulation results in Table 2, a 3D model of Au−TTF was obtained where the molecules were oriented according to the Euler angles and the angle ψ between two molecular planes (molecule A and B) (as shown in Figure S10, Supporting Information). This is in contrast to the proposed molecular mechanism in previously reported work,[6] which assumed a uniform orientation of partially charged TTF^{n+} ($0 < n < 1$) molecules in Au−TTF nanowires (Figure 4a). In our work, to the contrary, two molecular orientations are found, with the angle (ψ) between the two different molecular planes being about $53.9 \pm 1.6°$, while the angle (A_w) of molecule A (red Y axis) to the longitudinal axis of the wire (blue X') is $19.9 \pm 1.3°$ (Table 2). This is illustrated in the 2D view of Au−TTF nanowire in Figure 4b.

On the basis of these results, the biaxial stacking mode of partially charged TTF^{n+} ($0 < n < 1$) molecules to form Au−TTF nanowires is shown in Figure 4c. With this mode, the growth of the Au−TTF nanowires can be well explained: the kinetic axial and radial growth happens at the same time. With the tilt angle of the molecules with respect to the nanowire long axis, partially charged TTF molecules can assemble along the long axis X' of

the wire and the stacking of these molecules leads to a growth of wire in length; on the other hand,, these molecules can be stacked along wire radial directions Y'. The ratio between the two growth rates is up to the preparation conditions (e.g., microfluidic flow rates),[1,4,5] which results in the different lengths of Au−TTF wires with diameters ranging from nanometer to several micrometers (Figure S1, Supporting Information). Notably, the average angle between molecule A and molecule B in Au−TTF nanowires ($53.9 \pm 1.6°$, ψ in Table 2) is very close to the angle between TTF molecule in a neutral crystal ($52.59°$, Figure S2). However, it is evident that the molecules in nanowires are charged, as can be seen from the difference in the Raman spectra of the Au−TTF nanowires and the neutral TTF bulk crystal. Hence, a stacking of the molecules is necessary to create a sufficient π-orbital overlap. Combined with the tilted molecular orientation derived from Raman measurements, a molecular column stacking in Au−TTF nanowires can be proposed (Figure 4c) showing similar alignment of the molecules as in TTF bulk crystals (Figure 4d) but a different packing mode.

4. CONCLUSIONS

To conclude, the molecular orientations in a series of individual Au−TTF nano- and microwires have been successfully analyzed and related to the morphology of these wires. The results of polarization dependent Raman measurements and the simulations of depolarization ratio demonstrated the tilted stacking of partially charged TTF^{n+} ($0 < n < 1$) molecules, both being neither perpendicular nor parallel to the long axis in single Au−TTF wire structures. In addition, both the angle between two molecular planes and the tilt angle of the molecules with respect to the long axis of the wire were quantitatively determined. Thus, we conclude that the so far assumed model of a simple columnar packing of TTF along the wire axis in reported work is not applicable to explain the morphology of the Au−TTF wires. Although the function of gold clusters in the formation of Au−TTF is still unclear, the different morphologies of Au−TTF wires with various diameters and lengths in different synthesis

experiments can be qualitatively explained by the biaxial growth model.

■ ASSOCIATED CONTENT

ⓢ Supporting Information

The Supporting Information is available free of charge on the ACS Publications website at DOI: 10.1021/acs.jpcc.7b05924.

> Tables and figures showing the calculation of depolarization ratio; Raman tensors for TTF and TTF$^+$; X-ray crystal structure of single TTF crystals; angular based polarized Raman spectra of TTF crystals; equations of the simulation of depolarization ratio; assignments of Raman modes of TTF, TTF^{n+} ($0 < n < 1$), and TTF$^+$; angular based polarized Raman spectra of Au−TTF nanowires; Raman intensity curves of peaks at 1415 cm^{-1} for different Au−TTF nano/microwires; simulation of depolarization ratio of Au−TTF microwires; 3D model of single Au−TTF nanowire; and images of TTF crystal and Au−TTF nano/microwires (PDF)

■ AUTHOR INFORMATION

Corresponding Author

*(E.S.) Telephone: +49 (0)2 31.13 92-3552. Fax: +49 (0)2 31.13 92-3544. E-mail: eugen.speiser@isas.de.

ORCID ⓘ

Yanlong Xing: 0000-0002-1134-2917
Eugen Speiser: 0000-0001-7546-1141
Petra S. Dittrich: 0000-0001-5359-8403

Notes

The authors declare no competing financial interest.

■ REFERENCES

(1) Puigmartí-Luis, J.; Schaffhauser, D.; Burg, B. R.; Dittrich, P. S. A Microfluidic Approach for the Formation of Conductive Nanowires and Hollow Hybrid Structures. *Adv. Mater.* **2010**, *22*, 2255−2259.

(2) Liu, Y.; Ji, Z.; Tang, Q.; Jiang, L.; Li, H.; He, M.; Hu, W.; Zhang, D.; Jiang, L.; Wang, X.; et al. Particle-Size Control and Patterning of a Charge-Transfer Complex for Nanoelectronics. *Adv. Mater.* **2005**, *17*, 2953−2957.

(3) Xing, Y.; Esser, N.; Dittrich, P. S. Conductive Single Nanowires Formed and Analysed on Microfluidic Devices. *J. Mater. Chem. C* **2016**, *4*, 9235−9244.

(4) Cvetković, B. Z.; Puigmartí-Luis, J.; Schaffhauser, D.; Ryll, T.; Schmid, S.; Dittrich, P. S. Confined Synthesis and Integration of Functional Materials in Sub-nanoliter Volumes. *ACS Nano* **2013**, *7*, 183−190.

(5) Xing, Y.; Wyss, A.; Esser, N.; Dittrich, P. S. Label-Free Biosensors Based on *in Situ* Formed and Functionalized Microwires in Microfluidic Devices. *Analyst* **2015**, *140*, 7896−7901.

(6) Naka, K.; Ando, D.; Wang, X.; Chujo, Y. Synthesis of Organic-Metal Hybrid Nanowires by Cooperative Self-Organization of Tetrathiafulvalene and Metallic Gold via Charge-Transfer. *Langmuir* **2007**, *23*, 3450−3454.

(7) Zahn, D. R. T.; Gavrila, G. N.; Salvan, G. Electronic and Vibrational Spectroscopies Applied to Organic/Inorganic Interfaces. *Chem. Rev.* **2007**, *107*, 1161−1232.

(8) Wang, X.; Broch, K.; Scholz, R.; Schreiber, F.; Meixner, A. J.; Zhang, D. Topography-Correlated Confocal Raman Microscopy with Cylindrical Vector Beams for Probing Nanoscale Structural Order. *J. Phys. Chem. Lett.* **2014**, *5*, 1048−1054.

(9) Riele, L.; Buick, B.; Speiser, E.; Fimland, B.-O.; Vogt, P.; Richter, W. Epitaxial-Like Growth of Lead Phthalocyanine Thin Layers on GaAs(001). In *Epioptics 11. Proceedings of the 49th Course of the International School of Solid State Physics, Erice, Italy, Jul 19−25, 2010*; Antonio, C., Ed.; World Scientific Publishing Co. Pte. Ltd.: Singapore, 2012; p 16.

(10) Phaneuf-L'Heureux, A.-L.; Favron, A.; Germain, J.-F.; Lavoie, P.; Desjardins, P.; Leonelli, R.; Martel, R.; Francoeur, S. Polarization-Resolved Raman Study of Bulk-like and Davydov-Induced Vibrational Modes of Exfoliated Black Phosphorus. *Nano Lett.* **2016**, *16*, 7761−7767.

(11) Pauzauskie, P. J.; Talaga, D.; Seo, K.; Yang, P.; Lagugné-Labarthet, F. Polarized Raman Confocal Microscopy of Single Gallium Nitride Nanowires. *J. Am. Chem. Soc.* **2005**, *127*, 17146−17147.

(12) Fréchette, J.; Carraro, C. Resolving Radial Composition Gradients in Polarized Confocal Raman Spectra of Individual 3C-SiC Nanowires. *J. Am. Chem. Soc.* **2006**, *128*, 14774−14775.

(13) Saito, Y.; Verma, P. Polarization-Controlled Raman Microscopy and Nanoscopy. *J. Phys. Chem. Lett.* **2012**, *3*, 1295−1300.

(14) Singh, D.; Vikram, K.; Singh, D. K.; Kiefer, W.; Singh, R. K. Raman and DFT Study of Hydrogen-bonded 2- and 3-Chloropyridine with Methanol. *J. Raman Spectrosc.* **2008**, *39*, 1423−1432.

(15) Sandman, D. J.; Epstein, A. J.; Chickos, J. S.; Ketchum, J.; Fu, J. S.; Scheraga, H. A. Crystal Lattice and Polarization Energy of Tetrathiafulvalene. *J. Chem. Phys.* **1979**, *70*, 305−313.

(16) Wudl, F.; Kaplan, M. L.; Hufnagel, E. J.; Southwick, E. W. Convenient Synthesis of 1,4,5,8-Tetrahydro-1,4,5,8-tetrathiafulvalene. *J. Org. Chem.* **1974**, *39*, 3608−3609.

(17) Frisch, M. J.; Trucks, G. W.; Schlegel, H. B.; Scuseria, G. E.; Robb, M. A.; Cheeseman, J. R.; Scalmani, G.; Barone, V.; Mennucci, B.; Petersson, G. A., et al. *Gaussian 09*, Revision E. 01.; Gaussian Inc.: Wallingford, CT, 2009.

(18) Singh, D. K.; Asthana, B. P.; Srivastava, S. K. Modeling the Weak Hydrogen Bonding of Pyrrole and Dichloromethane Through Raman and DFT Study. *J. Mol. Model.* **2012**, *18*, 3541−3552.

(19) Lam, A. T.; Yoon, J.; Ganbold, E. O.; Singh, D. K.; Kim, D.; Cho, K. H.; Son, S. J.; Choo, J.; Lee, S. Y.; Kim, S.; et al. Adsorption and Desorption of Tyrosine Kinase Inhibitor Erlotinib on Gold Nanoparticles. *J. Colloid Interface Sci.* **2014**, *425*, 96−101.

(20) Berlinsky, A. J.; Hoyano, Y.; Weiler, L. Raman Spectra of Tetrathiofulvalene (TTF). *Chem. Phys. Lett.* **1977**, *45*, 419−421.

(21) Mukherjee, V.; Singh, N. P. Theoretical Vibrational Spectra and Thermodynamics of Organic Semiconductive Tetrathiafulvalene and Its Cation Radical. *Spectrochim. Acta, Part A* **2014**, *117*, 315−322.

(22) Cooper, W. F.; Kenny, N. C.; Edmonds, J. W.; Nagel, A.; Wudl, F.; Coppens, P. Crystal and Molecular Structure of the Aromatic Sulphur Compound 2,2′-Bi-1,3-dithiole. Evidence for D-Orbital Participation in Bonding. *J. Chem. Soc. D* **1971**, *0*, 889−890.

(23) Lovrinčić, R.; Trollmann, J.; Pölking, C.; Schöneboom, J.; Lennartz, C.; Pucci, A. Orientation of Nonplanar Molecules in Polycrystalline Layers from Infrared Spectra: Core-Chlorinated Naphthalene Tetracarboxylic Diimides. *J. Phys. Chem. C* **2012**, *116*, 5757−5763.